Electrochimica Acta 54 (2009) 1826–1833

Contents lists available at ScienceDirect

Electrochimica Acta

journal homepage: www.elsevier.com/locate/electacta

The effect of humidity and oxygen partial pressure on degradation of Pt/C catalyst in PEM fuel cell

Wu Bi[a,*], Qunhui Sun[a,b], Yulin Deng[a,b], Thomas F. Fuller[a,c]

[a] School of Chemical & Biomolecular Engineering, Georgia Institute of Technology, Atlanta, GA 30332, United States
[b] IPST, Georgia Institute of Technology, Atlanta, GA 30332, United States
[c] Center for Innovative Fuel Cell and Battery Technologies, Georgia Tech Research Institute, Georgia Institute of Technology, Atlanta, GA 30332, United States

ARTICLE INFO

Article history:
Received 16 July 2008
Received in revised form 7 October 2008
Accepted 7 October 2008
Available online 18 October 2008

Keywords:
Fuel cell platinum catalyst degradation
Platinum oxidation and dissolution
Pt ion diffusivity
Relative humidity
Oxygen partial pressure

ABSTRACT

Durability of Pt/C oxygen reduction reaction (ORR) catalyst remains one of the primary limitations for practical application of proton exchange membrane (PEM) fuel cells. In this work, the effects of relative humidity and oxygen partial pressure on platinum catalyst degradation were explored under potential cycling. At 60 °C, the loss rates of Pt mass and catalyst active surface area were reduced by about three and two times respectively when the relative humidity was lowered from 100% to 50%. The effects of oxygen partial pressure on cathode degradation were found to be insignificant. Cyclic voltammetry studies showed a slight increase in Pt electrochemical oxidation by water when the humidity increased from 50% RH to 100% RH. The rates of Pt dissolution were only slightly affected by change in humidity, and the accelerated catalyst degradation was ascribed to the increased Pt ion transport in the more abundant and larger water channel networks within the polymer electrolyte. Based on the parametric study results from our previous cathode degradation model, it was estimated that the diffusivity of Pt ions at fully humidified conditions was three times that of the value at 50% RH and 60 °C.

1. Introduction

Although many technical advancements have been made in theoretical understanding, materials design/preparation, and systems engineering of fuel cells over the last decade, durability of proton exchange membrane (PEM) fuel-cell components, including the platinum catalyst for oxygen reduction reaction (ORR), remains one of the primary limitations for commercialization. The fuel-cell cathode is subjected to frequent potential oscillation in transportation applications, such as in fuel cell or fuel-cell hybrid vehicles. Research efforts to understand better the degradation processes of fuel-cell components, including the most common ORR catalyst of carbon-supported platinum nanoparticles, are important and necessary. This understanding provides future guidance to design more durable materials and to prolong fuel-cell lifetimes.

In general, the formation of soluble platinum under the combined electrochemically oxidizing and acidic environment causes degradation of cathode Pt/C catalyst. A decrease in electrochemical active surface area (ECA) and the growth of Pt particles with broadened size distributions result from the following processes: (1) transport of soluble Pt species in the MEA components; and (2) Pt ions re-deposition by electrochemical reduction at solid phase surfaces (carbon support and/or Pt particles) and in some situations chemical reduction by hydrogen that permeates in the polymer electrolyte phase. Hence, the cathode overpotential increases and the overall cell performance decreases during cell lifetime tests or accelerated durability tests. An increase of cathode potentials up to 1.1 V (vs. SHE) will increase the concentration of dissolved Pt [1]. Further study of Pt dissolution and stability in perchloric acid at Argonne National Laboratory [2] found that the nanofaceted single-crystal surfaces with edges and corners had higher dissolution rates than the low-index surfaces, which was explained by the better Pt oxide passivation of the low-index surfaces. Previous studies of PEM fuel-cell durability including Pt based catalysts have been well reviewed by Borup et al. [3].

One active PEM fuel-cell research effort is the development of membranes for fuel-cell operations at high-temperature and low-humidity conditions. Operation at higher temperatures allows for better heat rejection and for simpler fuel-cell stack design. However, accelerated cathode catalyst degradation at high temperatures was observed in our previous study [4,5]. In Borup et al.'s brief study of Pt particle growth during durability tests [6], the growth rates were found to be accelerated at high cell potentials, increased cell temperatures, and high relative humidity conditions. Both humidity (water activity) and oxygen partial pressure are known to affect

* Corresponding author. Present address: UTC Power, 195 Governor's Hwy., South Windsor, CT 06074, United States. Tel.: +1 860 727 2137.
E-mail address: Wu.Bi@utcpower.com (W. Bi).

0013-4686/$ – see front matter © 2008 Elsevier Ltd. All rights reserved.
doi:10.1016/j.electacta.2008.10.008

platinum oxidation [7,8], which is an important process that influences the oxygen reduction activity and durability of catalysts. Increased surface oxide coverage of platinum nanoparticle is generally believed to reduce the ORR activity of the catalyst by blocking oxygen molecule adsorption sites [9] and to slow down platinum dissolution or degradation process [10–12]. It was found in Paik et al.'s study [7] that about 80% of oxide was formed through Pt oxidation by oxygen gas at the cathode potential of 0.85 V vs. reference hydrogen electrode (RHE) at 25 °C and 100% RH. In a more recent study by Xu et al. [8], a series of reactions were proposed for the oxidation of Pt by gaseous oxygen as shown below in reactions (1)–(4). It was also found that at 0.85 V vs. RHE, 50% of the oxide was formed from the electrochemical oxidation by water at 100 °C and 20% RH. The percentage of oxide formed from water increased to 70% at 100% RH. So as the temperature and humidity increased, platinum electrochemical oxidation by water became more important. On the other hand, the water content in the ionomer influences the rate of transport of Pt ions. The details of cation transport in Nafion® are still under investigation, but the conductivity depends strongly on the water content. Similarly, increased sorption of water in the membrane should increase the diffusivity of Pt ions, and consequently the rate of mass loss of platinum from the cathode into the membrane increases [12].

$$\mathrm{Pt} + \mathrm{O_2} \rightarrow \mathrm{Pt\text{-}O_2} \quad (1)$$

$$\mathrm{Pt\text{-}O_2} + \mathrm{H^+} + \mathrm{e^-} \rightarrow \mathrm{Pt\text{-}HO_2} \quad (2)$$

$$\mathrm{Pt\text{-}HO_2} + \mathrm{Pt} \rightarrow \mathrm{Pt\text{-}OH} + \mathrm{Pt\text{-}O} \quad (3)$$

$$\mathrm{Pt\text{-}OH} \rightarrow \mathrm{Pt\text{-}O} + \mathrm{H^+} + \mathrm{e^-} \quad (4)$$

In this work, we further explored the effects of relative humidity (or water activity) and oxygen partial pressure on the degradation of platinum supported on carbon, the standard PEM fuel-cell catalyst. The rates of dissolution were measured under accelerated cathode degradation conditions by potential cycling. Cyclic voltammetry (CV) experiments were also conducted at various temperature and relative humidity conditions to study platinum oxidation by water in non-reacting nitrogen environments. Parametric studies based on our previous cathode degradation model [12] were presented to elucidate the impact of metal dissolution and transport of Pt ions in membrane.

2. Experimental

As described elsewhere [4], commercial CCMs (1–6): 5 cm × 5 cm constructed from Nafion® 117 membrane and Pt/C catalyst layers with Pt loadings of 0.3 $mg_{Pt}\,cm^{-2}$ in both the anode and cathode were used. All CCMs were wet-up for 2 h and conditioned for total 24 h at three current densities in the order of 20, 100, and 200 $mA\,cm^{-2}$ with 8 h for each current holding. Following conditioning, the potential of the cell was cycled at a cell temperature of 60 °C with a square-wave between 0.87 and 1.2 V vs. reference hydrogen electrode and a time step of 30 s at each potential, using a Potentiostat/Galvanostat (EG&G Princeton Applied Research 273A). Pure hydrogen (0.38 $dm^3\,min^{-1}$) was supplied to the anode, which served as both the reference and the counter electrodes. Pure N_2 (CCM 1–2), air (CCM 3–4), or pure oxygen (CCM 5–6) was supplied to the cathode, the working electrode, at a flow rate of 0.91 $dm^3\,min^{-1}$. The temperatures of both anode and cathode saturators were set to be 45.8 °C (50% RH for tests of CCM 2, 4, and 6) or 60 °C (100% RH for tests of CCM 1, 3, and 5). The potential was cycled a total of 3600 times, and during these tests the cathode ECAs were periodically measured with liquid water in the working electrode. The RHE potential difference between the two humidity conditions was 1.6 mV due to slight changes in hydrogen partial pressure. Based on our catalyst degradation model [12], this small potential shift resulted in a less than 1% difference of the initial catalyst degradation rates. The degraded CCMs were all observed by SEM/EDS to study the distributions of Pt catalyst at the CCM cross-sections with the surface coated Au as the reference element [13]. The Pt particle sizes and size spatial distributions in the degraded CCMs (anode catalyst carefully scratched off) were studied by X-ray diffraction with a fixed incidence angle [4]. Only Pt {1 1 1} peak from 35° to 44° of 2θ was measured, and the volume-averaged Pt crystal size was estimated by fitting the peak in Jade 7.5 (Material Data, Inc.). Due to X-ray relative intensity decay, the incidence angle was varied from 0.5° to 20° to probe the platinum particles in the cathode and/or the deposited Pt particles in the membrane during degradation procedures. A high incidence angle allowed deep penetration of the X-ray into the sample and the easy detection of deposited Pt particles in the membrane. Also the deposited Pt particles in the membrane of CCM 3 were observed on a JEOL 100C Transmission electron microscopy (TEM) with an accelerating voltage of 100 kV. The sample was embedded within an epoxy resin matrix and the ultratoming was conducted on a Leica Ultracut R machine. The ultra-thin cut films were about 70 nm thick and were directly transferred onto the TEM grid for observation.

To quantify the effects of humidity on Pt electrochemical oxidation by water, cyclic voltammetry curves were measured in the potential range of 20–1000 mV (vs. RHE) with a scan rate of 50 $mV\,s^{-1}$ under the varied cell temperatures (40–80 °C) and humidity conditions (30–100% RH). Pure hydrogen and nitrogen at atmospheric pressures were provided to the anode and the cathode, respectively. The charge associated with Pt oxidation of the entire electrode (25 cm^2) was calculated by integrating the oxidation peak areas with the charging/de-charging current and the hydrogen crossover current removed. Due to the some overlapping of the hydrogen adsorption peak and the hydrogen evolution peak when using nitrogen at the working electrode, the electrochemically active surface areas were reported as the average value from hydrogen adsorption (integration down to 60 mV vs. RHE) and hydrogen desorption peak areas with a catalyst loading of 0.3 $mg_{Pt}\,cm^{-2}$. The Pt oxidation charges were normalized with the active surface area.

3. Results and discussion

3.1. Catalyst ECAs

The active surface areas decreased during the cathode degradation tests as shown in Fig. 1. All CCMs had high initial active surface areas ($S0$) of 105–135 $m^2\,g^{-1}$ Pt with an average Pt particle size ($D0$) of 2.2 nm diameter determined from XRD. The ECAs plotted in Fig. 1 show a 1st order loss rate (Eq. (1′)) with number of potential cycles (N) similar to our previous observations [4]. The relative humidity effect on the catalyst active surface area loss was quite clear. All three tests conducted at 100% RH had much higher loss rates of active surface area than their lower humidity counterparts. The fitted rate constant of the average surface loss (k_S) was 2.05×10^{-4} and 3.72×10^{-4} $cycle^{-1}$ (or min^{-1}) at 50% RH and 100% RH respectively. On the other hand, the partial pressure of oxygen only had a minor effect, with a very slightly lower ECA loss rate at a higher oxygen partial pressure, possibly due to the slightly higher Pt oxide surface coverage.

$$\frac{dS(N)}{dN} = -k_S \times S(N) \quad \text{or} \quad \ln\left[\frac{S(N)}{S0}\right] = -k_S \times N \quad (1')$$

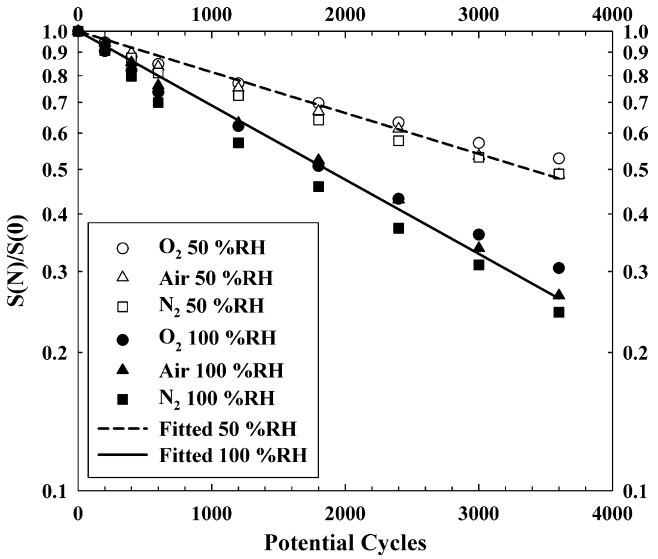

Fig. 1. Active surface area losses on cathode during the potential cycling at 60 °C.

3.2. Pt distributions at the CCM cross-sections

The cross-sections of all degraded CCMs were observed by SEM, and the images are shown in Fig. 2. Flowing air (CCMs 3–4) or pure oxygen (CCMs 5–6) at the cathode resulted in Pt band formation in the membrane with the location depending on the rates of gas permeations as described in previous studies [13,14]. As expected, there was no Pt band in CCMs 1–2 with nitrogen flowing at the cathode.

Pt element SEM/EDS line scans around the degraded CCMs 1–2 cathodes, shown in Fig. 3, confirmed the Pt deposition at the cathode-membrane interface with nitrogen at the cathode. And it is clear that there was significantly greater deposition of Pt under fully humidified condition (CCM 1) compared to the low-humidity case (CCM 2). The estimated amounts of Pt deposited in the Pt bands (CCMs 3–6) are listed in Table 1. Similar to the loss rate of catalyst active surface, the Pt mass losses at high humidity conditions were more than double those measured at the low-humidity condition. Again, no large differences in the loss of Pt from the cathode were observed between air and pure oxygen tests for both high and low-humidity conditions.

3.3. Pt particle sizes

The Pt particle sizes in the degraded CCMs were measured by X-ray diffraction with the copper anode Kα radiation. To probe the Pt particle sizes at the cathodes, the cathode/membrane interfaces, and/or the Pt bands in the membrane, the X-ray incidence angle was varied from 0.5° to 20°. To estimate the X-ray penetration depth in a fresh CCM, relative intensities of the incidence X-ray were calculated (Eq. (2′)) with the penetration distances (x) from the cathode surface. The mass attenuation coefficients (μ/ρ) and density (ρ) of the electrode and the membrane (Nafion® 1100) were calculated (Table 2) based on elemental mass attenuation coefficients [15] weighted by element percentages. The electrode contained 30 wt.% Nafion® 1100 polymer and Pt supported on Vulcan carbon (20 wt.% of Pt in Pt/C). The Nafion® polymer was simply assumed to have a composition of CF_2 neglecting the elements of sulfur and oxygen. The Pt catalyst loading in the electrode was 0.3 $mg_{Pt}\,cm^{-2}$ (14 wt.% Pt in electrode), and the total electrode mass (0.3/14% mg cm^{-2}) divided by the electrode thickness of 10 μm gave the estimated overall electrode density about 2.14 g cm^{-3}. The density of air-dried Nafion® 1100 is about 1.95 g cm^{-3} [16].

$$\frac{I(x)}{I_0} = \exp\left[-\left(\frac{\mu}{\rho}\right)\rho x\right] \quad (2')$$

The calculated X-ray relative intensity profiles with the vertical penetration distance from a fresh cathode surface are plotted in Fig. 4. With an incidence angle of less than 2°, only the

Table 1
Platinum distributions in a fresh and the degraded CCMs.

CCMs/regions		Pt/Au ratio	Width (μm)	Estimated CCM Pt %	Cathode Pt mass loss %
Fresh CCM	Cathode	1.10 ± 0.07	10.7 ± 1.6	50.7	
	Anode	1.09 ± 0.03	11.1 ± 1.0	49.3	
CCM 3 (H_2/air 100% RH)	Cathode	0.9 ± 0.1	11.3 ± 0.5	33.7	
	Pt band	5.2 ± 0.5	0.8 ± 0.1	14.5	30
	Anode	1.3 ± 0.3	11.5 ± 0.5	51.8	
CCM 4 (H_2/air 50% RH)	Cathode	1.1 ± 0.3	12.5 ± 0.4	44.5	
	Pt band	2.6 ± 0.5	0.66 ± 0.04	5.9	11
	Anode	1.2 ± 0.2	12.8 ± 0.6	49.7	
CCM 5 (H_2/O_2 100% RH)	Cathode	0.57 ± 0.05	10.3 ± 0.6	33.9	
	Pt band	1.85 ± 0.29	1.3 ± 0.2	13.9	29
	Anode	0.88 ± 0.04	10.5 ± 1.6	52.3	
CCM 6 (H_2/O_2 50% RH)	Cathode	1.3 ± 0.4	9.6 ± 0.6	44.3	
	Pt band	1.7 ± 0.4	1.0 ± 0.1	6.0	12
	Anode	1.4 ± 0.3	10.0 ± 1.0	49.7	

Table 2
Calculated cathode and membrane mass attenuation coefficients in a fresh Nafion® 117 CCM under the Cu Kα line (8.0478 kV) radiation.

Regions	Elements	Element mass attenuation coefficients ($cm^2\,g^{-1}$)	Element weight percentages (%)	Products	Weighted mass attenuation coefficients ($cm^2\,g^{-1}$)
Cathode	C	4.505	60	2.703	34.24
	F	15.77	26	4.100	
	Pt	196.0	14	37.44	
Membrane	C	4.505	14	0.631	14.19
	F	15.77	86	13.562	

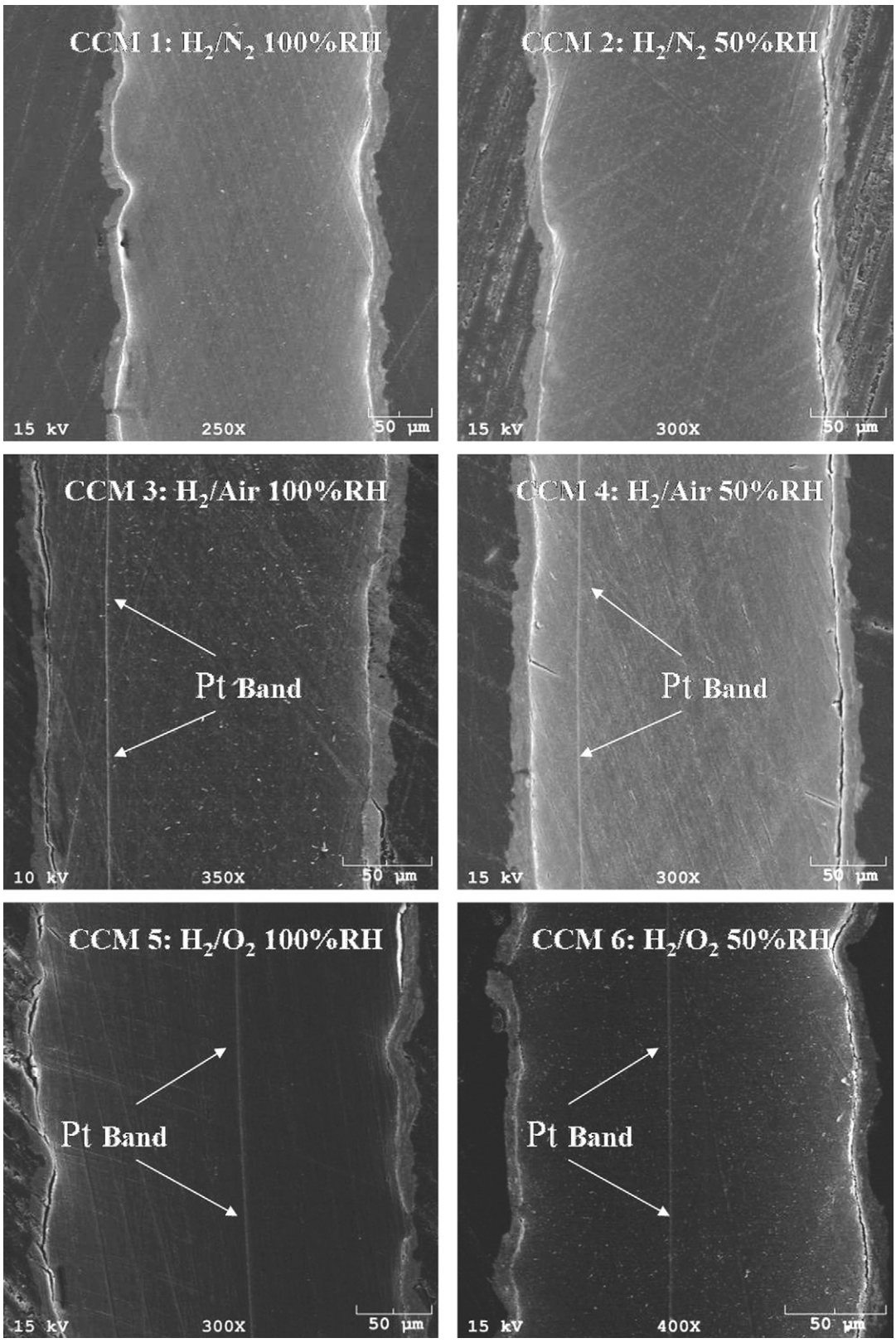

Fig. 2. SEM images of the degraded CCMs cross-sections (all cathodes on the left).

cathode region is subjected to the X-ray detection. At high angles of incidence, Pt particles deposited in the membrane (30 μm or 90 μm beneath the cathode/membrane interface for the H_2/air or H_2/O_2 cycled CCMs) can be detected depending on the particle abundance (or Pt element content) and particle sizes.

The fitted Pt particle sizes from Pt {1 1 1} peaks are plotted in Fig. 5. For the H_2/N_2 cycled CCMs 1–2, platinum amounts were not

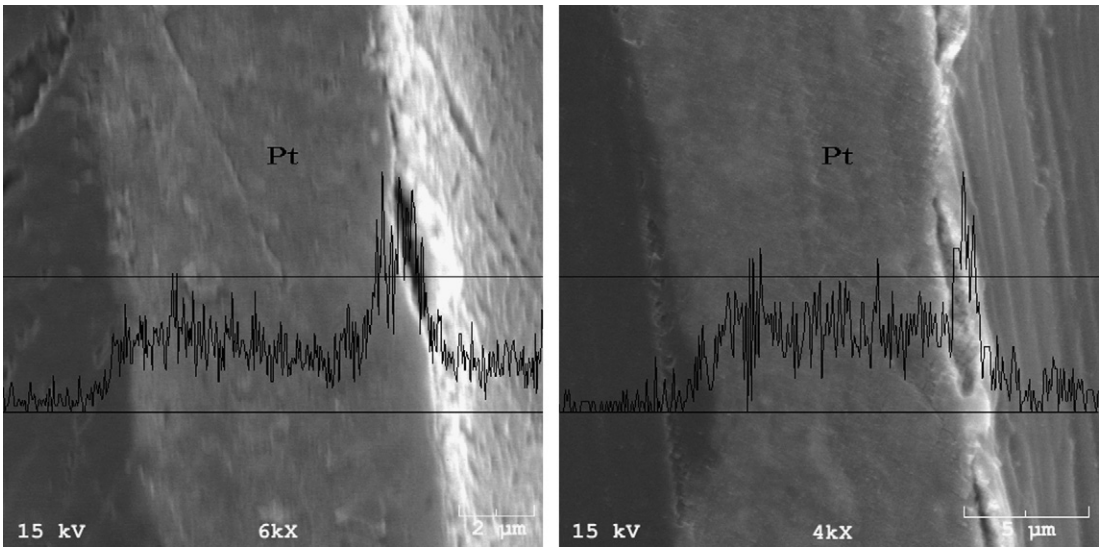

Fig. 3. SEM line scans of Pt element content in the degraded cathodes: CCM 1, N_2 and 100% RH (left); CCM 2, N_2 and 50% RH (right).

uniformly distributed in the cathode region. A significant amount of Pt is deposited at the interface as shown in Fig. 3. Pt particles sizes (CCMs 1–2) determined from the X-ray measurements generally increased with increasing X-ray incidence angle. Although the measured Pt particles size is the averaged value depending on Pt content, particle sizes, and X-ray intensities over the whole detectable region, it was evident that Pt particles deposited at the interface were much larger than those in the cathode. Similar large size of Pt particles (about 30 nm) deposited in the ionomer was observed by TEM images in a H_2/N_2 degraded CCM cathode/membrane interface [17]. For the H_2/air (or pure oxygen) cycled CCMs, the measured Pt particle sizes were relatively uniform with an incidence angle of 0.5–2°. As the X-ray angle of incidence was increased further, Pt particles in the "Pt band" were detected as shown by the significant increase of measured Pt particle size. The deposited Pt particles in CCM 3 membrane were observed by TEM as shown in Fig. 6 with the average particle sizes of 40–50 nm, which were comparable to the XRD measured value at the high incidence angles.

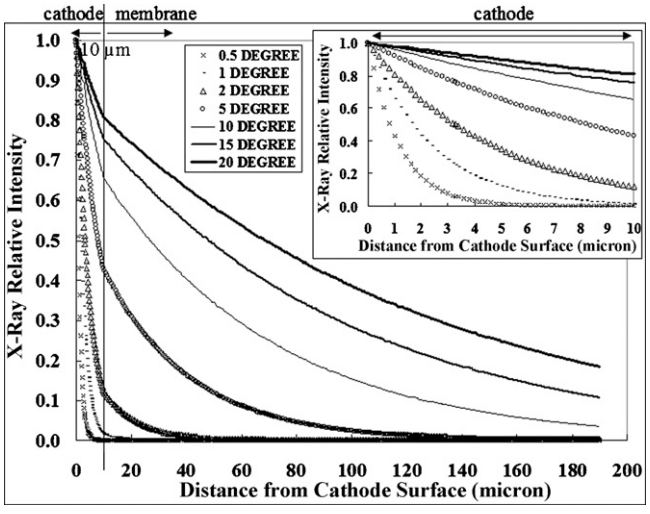

Fig. 4. Calculated X-ray relative intensities with vertical distances from cathode surface into a fresh Nafion® 117 CCM at the varied incident angles.

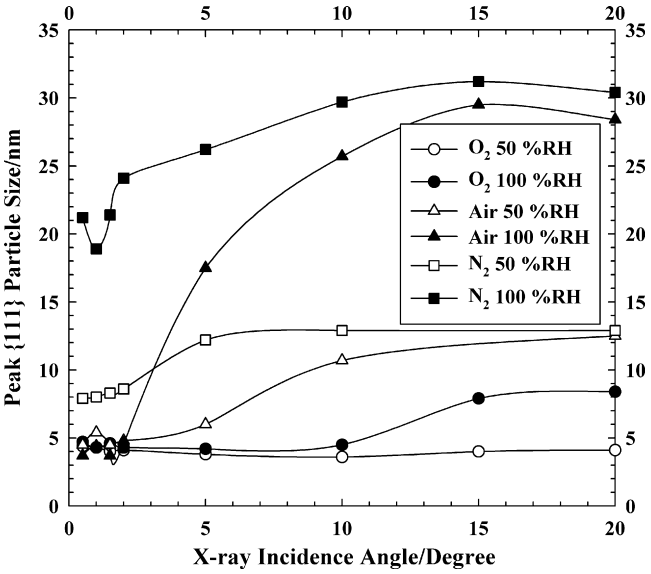

Fig. 5. Pt particle sizes in the degraded CCMs at varied X-ray incident angles.

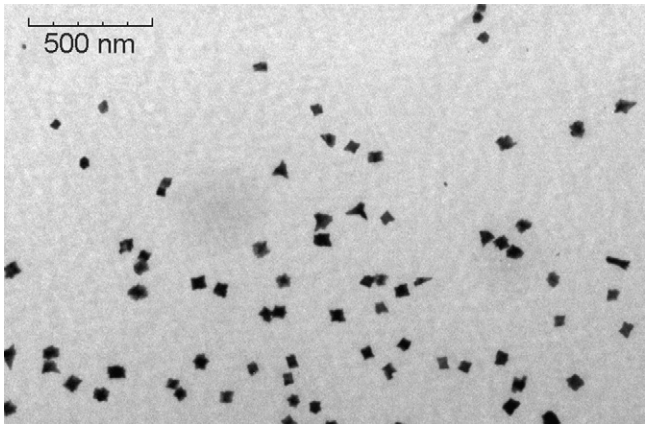

Fig. 6. TEM image of the deposited Pt particles in CCM 3 membrane.

Comparing pairs of high and low-humidity conditions, the measured particle sizes at high incidence angles were quite different. This was due to more deposition of Pt at the interface or in the membrane confirmed by SE/EDS studies and possible increased size of deposited particles with cathode Pt mass loss. However, in the cathodes (with the incidence angles of smaller than 2°) under H_2/air (or O_2) cycling conditions, no significant Pt particle size differences were observed.

3.4. Cathode platinum mass loss rate

With the measured catalyst particle sizes, active surface areas, and Pt masses, the loss rates of Pt mass from the cathode were calculated with the number of potential cycles N. It was simply written that the mass loss rate was proportional to active surface area $S(N)$ and catalyst loading CL (7.5 mg_{Pt} per cathode). The exponential term of the inverse of particle size [4] was included due to the concern of particle size effects on Pt dissolution rate in a form of Butler–Volmer equation. σ is the surface tension (2.37 J mol^{-1}) [18], M is the Pt molecular weight (195.1 g mol^{-1}), ρ_{Pt} is the Pt metal density (21.45 g cm^{-3}), and k' (g cm^{-2} Pt min^{-1} or g cm^{-2} Pt $cycle^{-1}$) is the fitted constant. The measured data of cathode Pt masses, particle sizes, and catalyst active surface areas were averaged from the tests with air and oxygen at each relative humidity level. Linear profiles of the averaged particle size $D(N)$ and active surface area $S(N)$ were assumed between two experimental measurements. The calculated Pt mass loss rate constant ($k'\, e^{(1/RT)(\sigma M/\rho_{Pt})(1/D(N))}$; g cm^{-2} Pt min^{-1} or g cm^{-2} Pt $cycle^{-1}$) was plotted in Fig. 7 with the fitted k' value of 2.87×10^{-12} and 7.84×10^{-12} (g cm^{-2} Pt min^{-1}) at 50% RH and 100% RH respectively. Fig. 7 shows that high humidity accelerated cathode Pt mass loss with the initial loss rate close to three times of the rate at the low-humidity condition. The positive humidity effects could result from accelerated Pt dissolution and/or Pt ion transport process, which are discussed further below. The Pt mass loss rates decreased with potential cycling due to increased stability with particle growth.

$$\frac{dm_{Pt}}{dN} = k'\, e^{\frac{1}{RT}\frac{\sigma M}{\rho_{Pt}}\frac{1}{D(N)}} \times S(N) \times CL \qquad (3')$$

3.5. Platinum oxidation by cyclic voltammetry

High humidity or water activity enhances the Pt electrochemical oxidation process, which is expected to slow down the rate of catalyst degradation. However, this contradicts the observed behavior—accelerated degradation at higher humidity. To quantify the effects of humidity on platinum electrochemical oxidation by water, cyclic voltammetry curves were measured as described previously, and the normalized Pt oxidation charges are plotted in Fig. 8. The figure shows the notably positive effects of temperature and humidity on platinum electrochemical oxidation. These results may help to explain the observations by Paik et al. [7] and Xu et al. [8] that higher temperature and higher humidity resulted in greater importance of electrochemical oxidation by water over gaseous oxygen. However, at 60 °C a humidity increase from 50% RH to 100% RH only resulted in about a 20% increase of normalized oxidation charge. Also, at a fixed total pressure, an increase of relative humidity decreased the oxygen partial pressure by about 10%, which should slow down Pt oxidation by gaseous oxygen. Hence, we believed that Pt surface oxide coverage under these two humidity levels at 60 °C was only slightly different.

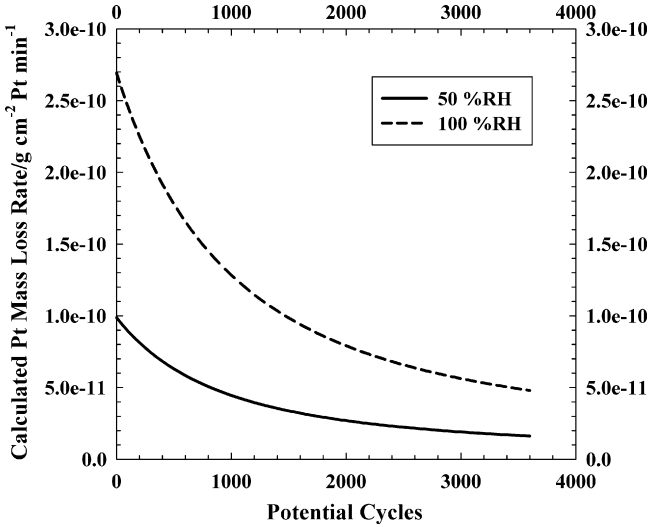

Fig. 7. Calculated Pt mass loss rate with number of potential cycles.

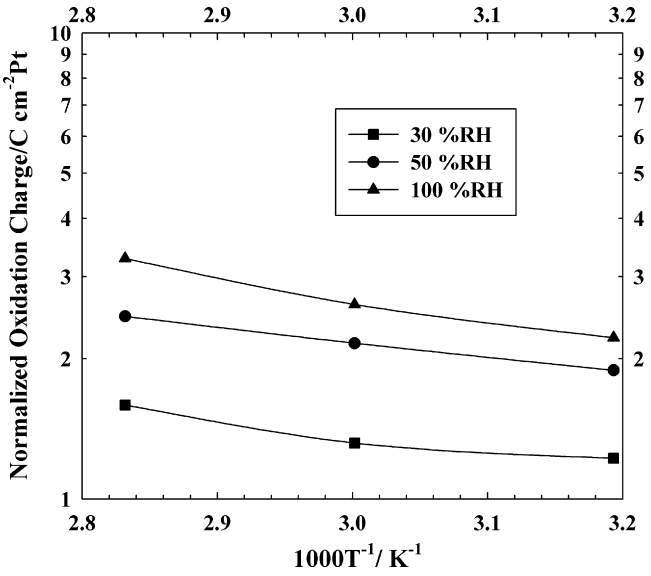

Fig. 8. Normalized Pt oxidation charge density vs. relative humidity.

3.6. Cathode degradation model parametric study and Pt ion diffusivity

A parametric study of the cathode degradation rates using our previous cathode degradation model [12] was conducted. The diffusivity of Pt ions was varied to observe the effects on catalyst degradation rates at the same electrochemical dissolution rate constant. In brief, the following processes were treated in the model: (1) electrochemical dissolution and re-deposition in the cathode; (2) Pt ion transport by diffusion in the MEA; and (3) Pt ion chemical reduction in membrane by hydrogen that permeates from the anode. A simplified bi-modal particle size distribution was adopted to simulate the overall cathode Pt particle growth, surface area loss and Pt mass loss. The model demonstrated that Pt dissolution and Pt ion deposition processes resulted in overall Pt particle growth by Pt mass exchange between small and large particles.

Utilizing the degradation model [12], the cathode degradation processes during the initial 200 potential cycles were simulated with air at a 5 cm × 5 cm cathode. The loss rates of Pt mass and surface area increased with the dissolution rate constant, k, and the diffusivity of Pt ions as shown in Figs. 9 and 10, respectively. For the overall particle growth, it was more complex as shown in Fig. 11. The rate of change in particle size (either growth or shrink-

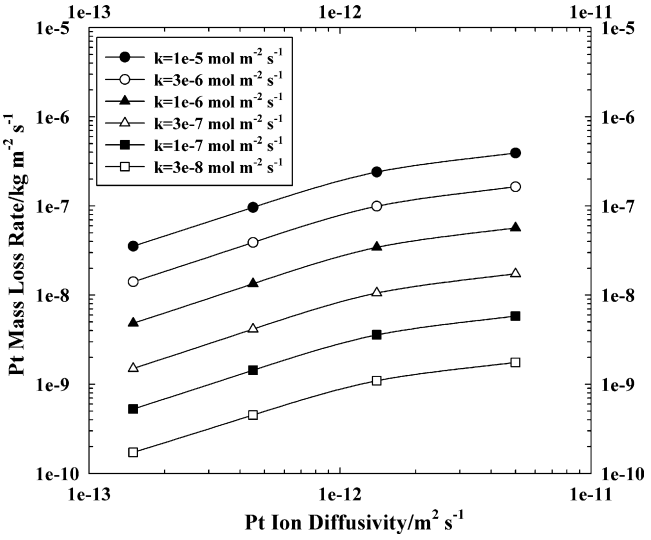

Fig. 9. Parametric study of initial cathode Pt mass loss rate during the square-wave potential cycling.

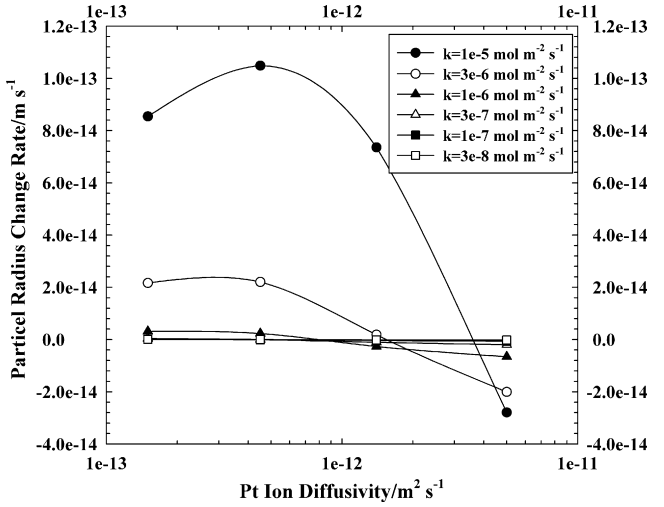

Fig. 11. Parametric study of initial cathode particle growth rate during the square-wave potential cycling.

age) increased with increasing Pt dissolution rate constant, k, or increasing concentration of Pt ions. Increased Pt ion diffusivity can initially increase the overall particle size growth rate due to the enhanced Pt mass exchange between small and large Pt particles, but eventually results in an overall particle size decrease due to the domination of Pt mass loss from the cathode over ripening.

As discussed previously, Pt oxidation may not be markedly different under the two humidity levels at 60 °C. Hence, the Pt dissolution rate should not change significantly with the change of relative humidity or surface oxide coverage. It was concluded in Okada's study that low water content in Nafion® resulted in low cationic mobility, depending on relative size of the moving cation and the ionic channel [19]. So the faster cathode degradation rates were ascribed to the accelerated Pt ion transport in polymer electrolyte at high humidity or high membrane water content due to most possible larger and more abundant water (and ionic) channel networks. Based on the observed initial cathode Pt mass loss rates and the catalyst active surface loss rates at two humidity levels in this work, parametric study results suggested that fitted Pt ion diffusivity at a fully humidified condition was about three times of the value at 50% RH with a cell temperature of 60 °C. This increase of the apparent Pt ion diffusivity seems reasonable considering other research results: a two–four fold increase of membrane water content [20,21] by mass or close to a three fold increase of water volume fraction (calculated by Eqs. (36) and (38) in [22]) with the humidity change from 50% to 100% between 30 and 80 °C. The water volume fraction can be viewed as a pre-factor to adjust the cation diffusivity [22] assuming the cation transport is limited to the hydrophilic regions of the polymer electrolyte. Also, a three fold increase of water diffusivity at 30 °C [20] and a five fold increase of proton conductivity at 60 °C [23] observed in literature were similar to the humidity effects on the Pt ion diffusivity in the polymer electrolyte.

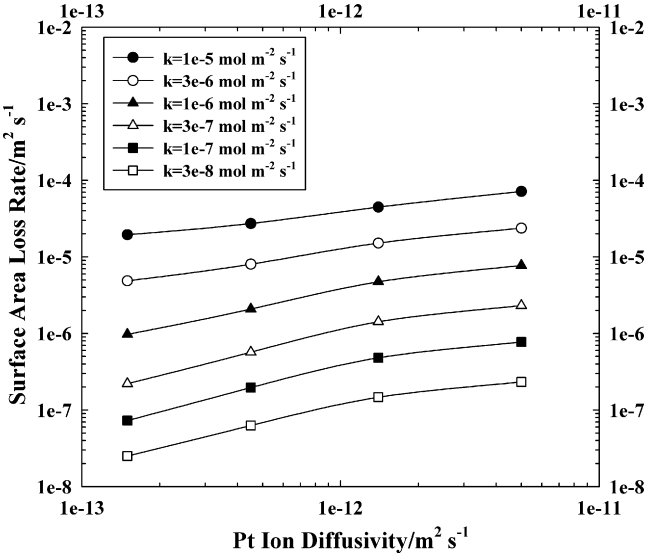

Fig. 10. Parametric study of initial cathode surface area loss rate during the square-wave potential cycling.

4. Conclusions

It was observed that cathode Pt catalyst degradation processes were accelerated with relative humidity increase. The loss rate of the cathode Pt mass and catalyst active surface area at 100% RH was about three and two times of that at 50% RH with the cell temperature of 60 °C, respectively. The effects of oxygen partial pressure on cathode degradation were found to be insignificant. When relative humidity increased, Pt electrochemical oxidation by water slightly increased and chemical oxidation by gaseous oxygen might decrease due to the reduced oxygen partial pressure. We believed that Pt surface oxide was not largely different at the two humidity levels. So Pt dissolution rate should not be significantly affected by the humidity change in our accelerated catalyst durability tests. Hence, the accelerated catalyst degradation was ascribed to the increased Pt ion transport in more abundant and larger water channel networks within polymer electrolyte. Based on the parametric study results from our previous cathode degradation model, it was estimated that the fitted Pt ion diffusivity at fully humidified condition was about three times of the value at 50% RH at 60 °C.

Acknowledgements

This work was supported by the Toyota Motor Engineering & Manufacturing North America, Inc. Also thanks to Mr. Cheng Chen, Mr. Kevin Gallagher, Ms. Rajeswari Chandrasekaran, and Mr. Norimitsu Takeuchi for the discussion of this work.

Appendix A. Nomenclature

CL	Pt loading in the cathode, 12.5 mg or 0.0125 g
$D0$	initial Pt particle diameter, nm
$D(N)$	Pt particle diameter during potential cycling, nm
F	Faraday's constant, 96,487 C eq^{-1}
k	Pt electrochemical dissolution rate constant in the degradation model, mol m^{-2} s^{-1}
k_S	fitted catalyst active surface area loss rate constant, $cycle^{-1}$
k'	fitted Pt mass loss rate constant, g cm^{-2} Pt $cycle^{-1}$
m_{Pt}	Pt mass in the cathode during potential cycling, g
M	Pt molecular weight, 0.1951 kg mol^{-1}
N	number of potential cycles
R	universal gas constant, 8.314 J mol^{-1} K^{-1}
$S0$	initial cathode ECA, m^2 g^{-1} Pt
$S(N)$	cathode ECA during potential cycling, m^2 g^{-1} Pt
T	temperature, K
x	X-ray vertical penetration distances from the cathode surface, μm

Greek letters

μ/ρ	cathode or Nafion® 1100 membrane mass attenuation coefficients, cm^2 g^{-1}
ρ	density of cathode or, g cm^{-3}
ρ_{Pt}	density of platinum, 21.45 g cm^{-3} or 21,450 kg m^{-3}
σ	surface tension of Pt nanoparticle, 2.37 J mol^{-1}

References

[1] X. Wang, R. Kumar, D.J. Myers, Electrochemical and Solid-State Letters 9 (2006) A225.
[2] V. Komanicky, K.C. Chang, A. Menzel, N.M. Markovic, H. You, X. Wang, D. Myers, Journal of The Electrochemical Society 153 (2006) B446.
[3] R. Borup, J. Meyers, B. Pivovar, Y.S. Kim, R. Mukundan, N. Garland, D. Myers, M. Wilson, F. Garzon, D. Wood, P. Zelenay, K. More, K. Stroh, T. Zawodzinski, J. Boncella, J.E. McGrath, M. Inaba, K. Miyatake, M. Hori, K. Ota, Z. Ogumi, S. Miyata, A. Nishikata, Z. Siroma, Y. Uchimoto, K. Yasuda, K.-i. Kimijima, N. Iwashita, Chemical Review 107 (2007) 3904.
[4] W. Bi, T.F. Fuller, Journal of the Electrochemical Society 155 (2008) B215.
[5] W. Bi, T.F. Fuller, ECS Transactions 11 (Proton Exchange Membrane Fuel Cells 7, Part 2) (2007) 1235.
[6] R.L. Borup, J.R. Davey, F.H. Garzon, D.L. Wood, M.A. Inbody, Journal of Power Sources 163 (2006) 76.
[7] C.H. Paik, T.D. Jarvi, W.E. O'Grady, Electrochemical and Solid-State Letters 7 (2004) A82.
[8] H. Xu, R. Kunz, J.M. Fenton, Electrochemical and Solid-State Letters 10 (2007) B1.
[9] H. Xu, Y. Song, H.R. Kunz, J.M. Fenton, Journal of The Electrochemical Society 152 (2006) A1828.
[10] S. Kawahara, S. Mitsushima, K. Ota, N. Kamiya, ECS Transactions 3 (2006) 625.
[11] R.M. Darling, J.P. Meyers, Journal of the Electrochemical Society 152 (2005) A242.
[12] W. Bi, T.F. Fuller, Journal of Power Sources 178 (2008) 188.
[13] W. Bi, G.E. Gray, T.F. Fuller, Electrochemical and Solid-State Letters 10 (2007) B101.
[14] J. Zhang, B.A. Litteer, W.G.H. Liu, H.A. Gasteiger, Journal of The Electrochemical Society 154 (2007) B1006.
[15] J.H. Hubbell, S.M. Seltzer, National Institute of Standards and Technology, http://physics.nist.gov/PhysRefData/XrayMassCoef/tab3.html, 1996.
[16] K.J. Oberbroeckling, D.C. Dunwoody, S.D. Minteer, J. Leddy, Analytical Chemistry 74 (2002) 4794.
[17] P.J. Ferreira, Y. Shao-Horn, Electrochemical and Solid-State Letters 10 (2007) B60.
[18] R.M. Darling, J.P. Meyers, Journal of the Electrochemical Society 150 (2003) A1523.
[19] T. Okada, H. Satou, M. Okuno, M. Yuasa, Journal of Physical Chemistry, B 106 (2002) 1267.
[20] T.E. Springer, T.A. Zawodzinski, S. Gottesfeld, Journal of Electrochemical Society 138 (1991) 2334.
[21] J.T. Hinatsu, M. Mizuhata, H. Takenaka, Journal of The Electrochemical Society 141 (1994) 1493.
[22] A.Z. Weber, J. Newman, Journal of The Electrochemical Society 151 (2004) A311.
[23] T. Thampan, S. Malhotr, H. Tang, R. Datta, Journal of The Electrochemical Society 147 (2000) 3242.